Journal of Pharmaceutical and Biomedical Analysis 172 (2019) 243–252

Contents lists available at ScienceDirect

Journal of Pharmaceutical and Biomedical Analysis

journal homepage: www.elsevier.com/locate/jpba

Novel urchin-like FeCo oxide nanostructures supported carbon spheres as a highly sensitive sensor for hydrazine sensing application

D.M. Nguyen [a], L.G. Bach [b], Q.B. Bui [c,*]

[a] Institute of Research and Development, Duy Tan University, Da Nang, 550000, Viet Nam
[b] Center of Excellence for Green Energy and Environmental Nanomaterials, Nguyen Tat Thanh University, Ho Chi Minh City, Viet Nam
[c] Sustainable Developments in Civil Engineering Research Group, Faculty of Civil Engineering, Ton Duc Thang University, Ho Chi Minh City, Viet Nam

ARTICLE INFO

Article history:
Received 9 November 2018
Received in revised form 23 March 2019
Accepted 6 April 2019
Available online 6 April 2019

Keywords:
Urchin-like nanostructure
Iron cobalt oxide
Carbon spheres
Electrocatalyst
Hydrazine detection
Biosensor

ABSTRACT

Herein, we successfully fabricated a novel nanostructure based on hierarchical urchin-like FeCo oxide supported carbon spheres (FeCo Oxide/CSs) via a two-step hydrothermal method followed by a simple annealing step at 300 °C under air. It was found that such urchin-like FeCo Oxide/CSs structure exhibited superior catalytic activity towards hydrazine oxidation to CSs, Fe Oxide/CSs, Co Oxide/CSs, and FeCo Hydroxide/CSs material. In this regard, the FeCo Oxide/CSs displayed a wide linear detection range of 0.1–516.6 μM, low detection limit of 0.1 μM, and long-term stability. The material also showed good selectivity towards hydrazine detection in the presence of various interferences, such as uric acid, ascorbic acid, urea, dopamine, Na^+, SO_4^{2-}, K^+, and Cl-. The excellent sensing performance of the FeCo Oxide/CSs was assumed to the unique hierarchical urchin structure with the high density and uniformity of nano-sized FeCo Oxide nanoneedles, which produced massive electroactive sites and enhanced charge transfer ability. The achieved results implied that the FeCo Oxide/CSs may be a great candidate for sensitive hydrazine detection.

1. Introduction

Hydrazine and its derivatives have been considered as the important substances for various applications, including pharmacy, energy conversion system, rocket, photo-printing, and agriculture [1]. Hydrazine appears under the form of colorless liquid, which is explosive, toxic, and combustible. This chemical is known to produce seriously negative influences for various human body's parts, such as lung, spleen, thyroid gland, central nervous system, and liver, thereby causing some risky diseases highly harmful towards our living quality [2,3]. Thus, preparation of efficient routes to determine hydrazine concentration at low concentration and wide range has been significantly required in industry and health care purposes. So far, many analytical methods, such as chemiluminescence, electrochemistry, spectrophotometry, chromatography, and potentiometry have been employed for sensing hydrazine [4–7]. As compared to these mentioned methods, electrochemical approach has proven with more benefits, including facile fabrication, excellent sensitivity, wide linear detection range, quick response time, and cost-effectiveness [8–11]. However, in order to achieve good efficiency of an electrochemical sensor, fabrication of working electrode via modification with specific electrocatalyst is necessary [12,13]. Recent researches have proposed various types of potential nanomaterials, including precious metals, non-precious metals, and the meta-carbon based hybrids [14–16]. Although the use of precious metals and their hybrids with carbon materials have provided good catalytic properties; however, the limited source and high cost hinder their practicality [17,18]. Meanwhile, transition metals have been recently emerging as the promising candidates for electrochemical applications, due to their abundance, low cost, high catalytic properties, and easy surface modification by reacting with various heteroatoms, such as O, N, C, P, and S [19–23]. In addition, the combination of two nonprecious metals to form a bimetallic alloy nanostructure has been reported as a promising way to impressively enhance catalytic activity and stability of the resulting material, as compared to mono-metal counterparts [24–28]. Because the formation of alloyed nanostructure can significantly modulate the electronic configuration and intrinsic properties of material, thereby resulting in the improved mechanical/chemical stability, outstanding electrical conductivity, poisoning/corrosion resistance, and excellent catalytic properties [29,30]. In this context, diverse bimetallic metal oxides have been employed and have proved better catalytic behavior or selectivity than a pure mono-metal oxide [31]; however, there is considerable gap to reach performance required for their real use in electrochemical biosensors.

* Corresponding author.
E-mail address: buiquocbao@tdtu.edu.vn (Q.B. Bui).

https://doi.org/10.1016/j.jpba.2019.04.008
0731-7085/

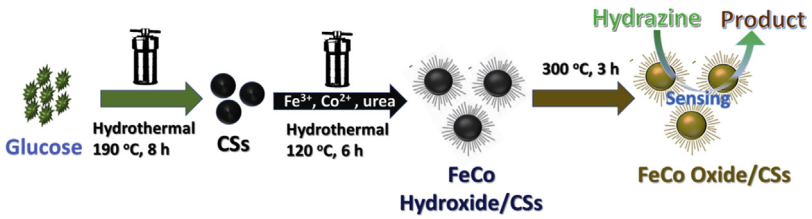

Fig. 1. The schematic illustration for the synthesis of FeCo Oxide/CSs hybrid.

Generally, the catalytic performance of the catalysts critically depends on the applied transition-metal precursors and preparation conditions. In addition, the use of a unique morphological and structural carbon-based support has been discovered to impressively enhance activity of active materials [32–35], due to the synergistic effects from components to improve electrical conductivity, surface chemistry, and active sites. Furthermore, a suitable carbon support can effectively stabilize the active metal catalysts under harsh working conditions by avoiding from the decomposition, agglomeration, and dissolution. Recent time, bimetallic catalysts of Co and Fe have been proposed to be very reactive for various electrochemical reactions due to their earth abundance, nontoxicity, and favorable bandgap [36–38]. Some literatures have reported transition metal oxides, including MnO_x, NiO_x, CoO_x, $NiFeO_x$, $FeCoO_x$ for diverse electrocatalytic oxidation reactions and they have demonstrated that the $FeCoO_x$ could yield earlier onset potential, smallest overpotential, highest turnover frequency, and the best current response [38–40]. These obtained results informed promising activity of the $FeCoO_x$ towards catalytic oxidation processes. However, its employment for catalyzing electrochemical oxidation of hydrazine in sensor development has not been reported to date. Therefore, the fabrication of a nanohybrid based on FeCo oxide with unique morphology and physicochemical properties is a necessary and useful approach to develop a new type of low-cost catalyst with the enhanced electrochemical activity for hydrazine detection. In this context, the hybridization of the FeCo catalysts with a suitable carbon substrate is also further expected to upgrade activity and stability of the material. The use of graphene (Gr) and carbon nanotubes (CNTs) has long been concerned as a highly efficient support, due to their excellent properties, such as high mechanical performance, superb conductivity, large surface area, and easy functionalization [41]. However, their complicated synthesis methods via wet chemical and chemical vapor deposition, substantially limit their applications. In addition to Gr and CNTs, carbon spheres (CSs) also has large surface area, high conductivity, functionalizable surface, but very facile synthesis [42,43]. Therefore, CSs has recently been emerging as a potential support for efficiently anchoring and promoting the homogeneous dispersion of active metals towards electrochemical reactions.

In this study, we successfully developed an urchin nanostructure of aligned FeCo nanoneedle arrays supported by CSs (FeCo Oxide/CSs) through a facile synthesis method. The hybrid demonstrated the enhancement of active surface area and electrical conductivity, thereby effectively serving as a biosensor for sensitively detecting hydrazine at low concentration. The high performance of the FeCo Oxide/CSs-based sensor implies that it can be a great potential for electrochemical sensing applications.

2. Experimental section

2.1. Chemicals

Cobalt nitrate hexahydrate ($Co(NO_3)_2.6H_2O$, 99.9%), ferric nitrate nonahydrate ($Fe(NO_3)_3.9H_2O$, 99.9%), hydrazine ($NH_2NH_2{\cdot}H_2O$, 98%), uric acid ($C_5H_4N_4O_3$, 99%), ascorbic acid ($C_6H_8O_6$, 99%), ethanol (C_2H_5OH, 99.5%), dopamine ($((HO)_2C_6H_3CH_2CH_2NH_2{\cdot}HCl$, 98%), urea ($CH_4N_2O$, 99%), sodium sulfate ($Na_2SO_4$, 99%), potassium chloride (KCl, 99%), sodium phosphate dibasic (Na_2HPO_4, 99%), and sodium phosphate monobasic (NaH_2PO4, 99%) were provided by Sigma-Aldrich Co. (USA).

2.2. Synthesis of FeCo Oxide/CSs hybrid

Prior to the preparation of FeCo Oxide/CSs hybrid, CSs was synthesized by a facile hydrothermal method. In this context, 4.0 g of glucose was dissolved in 30 ml DI water under sonication to produce a homogeneous solution. The solution was then put into a Teflon-lined autoclave, which was kept at 190 °C for 8 h. The resulting black-brown solid was washed with pure water and ethanol for several times before it was dried at 60 °C for 10 h under vacuum condition.

To fabricate FeCo Oxide/CSs, 30 ml of water containing 0.1 g of CSs was sonicated for 30 min followed by adding 0.9 mol of $Fe(NO_3)_3$, 0.9 mol of Co $(NO_3)_2$, and 0.75 g of urea under magnetic stirring. During this step, the presence of oxygen functional groups on CSs' surface made it become negative charged state [42,43], which easily adsorbed Fe^{3+} and Co^{2+} ions to form a layer of these positive ions on CSs' surface. After 30 min, the resulting solution was put into a Teflon-lined autoclave for a reaction at 120 °C for 6 h. Regarding this step, urea was degraded into NH^{4+} ions, which immediately reacted with Fe^{3+} and Co^{2+} on CSs' surface to produce an initial layer of FeCo hydroxide nanocrystals [44]. These nanocrystals displayed as nucleuses for the deposition of following Fe^{3+} and Co^{2+} ions to generate uniform FeCo hydroxide nanoneedles on CSs. After the reaction was completed, the precipitate was collected and washed with water/ethanol for 3 times and then dried for 24 h in vacuum. Finally, the achieved solid was kept in a small boat, which was positioned in a quenching machine under air atmosphere at 300 °C for 3 h. The purpose of this step was to convert FeCo hydroxide to oxide through a thermal reduction with the water removal. The system was cooled down to room temperature and the FeCo Oxide/CSs product was collected for next experimentations. All steps for the synthesis of the FeCo Oxide/CSs is schematically illustrated in Fig. 1. For a comparison, Co Oxide/CSs and Fe Oxide/CSs were also prepared with the same synthesis condition as mentioned above.

2.3. Material characterizations

The morphology of the as-synthesized materials was achieved by field emission scanning electron microscope (SEM) on a JSM 6600 (JEOL Co., Japan). Transmission electron microscopy (TEM) images achieved by a JEM-1400 Philips microscope (JEOL Co., Japan) were used to observe detail microstructure of materials. The Raman spectra of materials were obtained using a LabRAM HR Evolution Raman microscope (HORIBA Co., Japan). Powder X-ray diffraction (XRD) was measured on a D8 Advance diffractometer (Bruker Co., Germany) with the use of Cu-Kα target (λ = 0.154 nm) and the scanned 2θ range of 5–80° at a scan rate of 2 °C min^{-1}. The sur-

face area of materials was evaluated on an SA-9600 Series (HORIBA Co., Japan).

2.4. Electrochemical measurements

For detecting hydrazine substance, this study used a ZIVE SP2 2Amp electrochemical workstation (WonATech Co., Ltd., Korea) integrated with a three-electrode cell system. A 0.1 M phosphate buffer solution (PBS) was prepared from NaH_2PO_4 and Na_2HPO_4 and was used as electrolyte through all experiments. Ag/AgCl and Pt wire were applied as the reference and counter electrode, respectively. For preparing working electrode, 3 mg of catalyst powder was dissolved into 1 ml of ethanol under sonication for 2 min. Then 10 μL of the resulting suspension was dropped onto a cleaned surface of glassy carbon electrode (GCE, diameter of 3 mm). After that, the modified GCE was dried in air at room temperature for 5 h before it was used for electrochemical measurements. Electrochemical impedance spectroscopy (EIS) was employed to evaluate charge transfer resistance (R_{ct}) of the working electrode in nitrogen-saturated 0.1 M PBS solution. The hydrazine detection was investigated by cyclic voltammetry (CV) and amperometry (i–t) in 0.1 M PBS solution. The amperometric tests were employed by successive addition of different hydrazine concentrations into a stirring 0.1 M PBS solution and the steady state of current density at each addition time was noted.

For testing performance of the FeCo Oxide/CSs-based sensor towards hydrazine determination in real samples, river water was used. In this context, 0.5 ml of river water was diluted in 25 ml of 0.1 M PBS solution, which was then spiked with four different hydrazine concentrations. The known hydrazine concentration in these solutions was then detected by the developed sensor; and the relative standard deviation percentage (RSD%) and recovery (%) were recorded. All electrochemical measurements were performed at temperature of 25 ± 1 °C.

3. Results and discussion

3.1. Morphological characterization

Figure S1 shows the morphology of CSs material, which has spherical shape and relative uniformity, along with the diameter of around 0.8–1 μm. The morphological features of the as-prepared Co Oxide/CSs, Fe Oxide/CSs, and FeCo Oxide/CSs were initially investigated by FE-SEM. Fig. 2 shows these oxides exhibit urchin–shaped nanoarchitectures with diameter of 1.5–2.0 μm. The structures of Co Oxide/CSs and FeCo Oxide/CSs are fully covered by abundantly vertical and uniform nanoneedles with a diameter of around 50 nm (Fig. 2a, b, g, and h). Meanwhile, the Fe Oxide/CSs possess a little difference (Fig. 2d and e), in which the Fe Oxide structures appear as aligned nanorods rather nanoneedles, along with their bigger diameter than that of the Co Oxide and FeCo Oxide. The formation of these oxide structures is further indicated by EDAX investigation (Fig. 2c, f and i). The presence of the specific peaks correlated to elements of each oxide structure implies the successful preparation of Co Oxide/CSs, Fe Oxide/CSs, and FeCo Oxide/CSs via a facile synthesis route. The formation of the urchin-like structure is expected to produce large surface area with an excellent capacity for abundant active sites, thereby highly beneficial for catalytic reactions [45,46].

The morphology of the FeCo Oxide/CSs hybrid was further examined by TEM technique. The TEM images in Fig. 3a–c clearly show the creation of an urchin structure with the radially aligned nanoneedles. The detailed structural information was provided by higher magnification TEM image, which indicates the FeCo Oxide nanoneedles have the length in the range of ~400–500 nm and diameter of around 40–50 nm. These unique one-dimensional nanoneedles is expected to offer the enhanced surface area along with more active site number to improve the catalytic activity. The HR-TEM image apparently shows the lattice fringes of a crystalline mixture belonging to d(110) planes of Fe oxide [47] and d(220) of Co oxide structure [48] (Fig. 3d). The SAED pattern (Fig. 3e) clearly evidences the multicrystalline features of the obtained hybrid material. To further identify the homogeneous distribution of Fe, Co, and O in the nanoneedle of the urchin–shaped nanostructures, the STEM and its corresponding EDS color mapping analysis were carried out (Fig. 3f). The EDS mapping exhibits the uniform distribution of Fe, Co, and O throughout the nanoneedle nanostructure, clearly approving the well mixing of Fe, Co, and O to form a homogeneous mixture of oxide nanostructures.

3.2. XRD and BET analysis

Fig. 4a presents the XRD patterns for CSs, Fe Oxide/CSs, Co Oxide/CSs, and FeCo Oxide/CSs hybrid in the diffraction 2θ range of 5° to 80°. For all surveyed samples, a broaden peak at 2θ of ~21.7° arises from the CSs feature [49]. In the case of the Fe Oxide/CSs, the available diffraction peaks at 2θ of 24.2°, 33.1°, 35.7°, 40.8°, 49.4°, 54.1°, 62.6°, and 64.1° can be assigned to the d(012), d(104), d(110), d(113), d(024), d(116), d(213) and d(300) crystalline planes of the Fe_2O_3 structure, respectively [50]. Meanwhile, the XRD pattern of the Co Oxide/CSs presents various peaks at 2θ of 31.3°, 36.9°, 44.6°, 55.8°, 59.5°, and 65.3°, associated with d(220), d(311), d(400), d(422), d(511), and d(440) crystalline planes, respectively, confirming the formation of Co_3O_4 nanostructures [51]. Concerning the FeCo Oxide/CSs, its XRD pattern exists all specific peaks for both Fe_2O_3 and Co_3O_4 phases, indicating that such material simultaneously contains a mixture of two these crystalline phases in its structure [52].

For characterizing the surface area and porous characteristics of materials, nitrogen adsorption-desorption isotherms of the CSs, Fe Oxide/CSs, Co Oxide/CSs, and FeCo Oxide/CSs hybrid were investigated. All surveyed materials exhibit the type IV isotherm type, suggesting their typical mesoporous features [53]. The Brunauere Emmette Teller (BET) surface area of the FeCo Oxide/CSs was found to be 115 $m^2 g^{-1}$, much higher than that of CSs (10 $m^2 g^{-1}$), Fe Oxide/CSs (99 $m^2 g^{-1}$), Co Oxide/CSs material (36 $m^2 g^{-1}$) (Fig. 4b). Besides, its pore-size distribution mainly concentrates in the range of 2–7 nm (Inset in Fig. 4b), further indicating the mesoporous features of the FeCo Oxide/CSs. The large surface area along with high pore volume of the FeCo Oxide/CSs as compared to other materials importantly suggest the increase of the exposed active site for advanced catalytic activity.

3.3. Electrochemical sensing application

In this study, the FeCo Oxide/CSs-modified GCE was applied as working electrode for hydrazine detection. The CV was investigated in 0.1 M PBS solution with the absence and presence of 0.1 mM hydrazine, as shown in Fig. 5a. It can be recognized that there is a strong and sharp peak appearing at around 0.8 V in the availability of hydrazine, indicating such modified electrode effectively catalyzed the hydrazine oxidation. As a reference, the CV measurements of the CSs, Fe Oxide/CSs, Co Oxide/CSs, and FeCo Hydroxide/CSs-modified GCEs were also investigated. Mean the CV result of the CSs-modified GCE shows no oxidation phenomenon towards hydrazine oxidation, the Fe Oxide/CSs, Co Oxide/CSs, and FeCo Hydroxide/CSs-modified GCEs clearly present a current peak due to the oxidation of hydrazine (Fig. 5b). However, these peaks have lower current intensity and positive potential as compared to those of the FeCo Oxide/CSs, implying poorer electrocatalytic activity of Fe Oxide/CSs, Co Oxide/CSs, and FeCo Hydroxide/CSs material than FeCo Oxide/CSs. The high-efficient catalysis for hydrazine oxi-

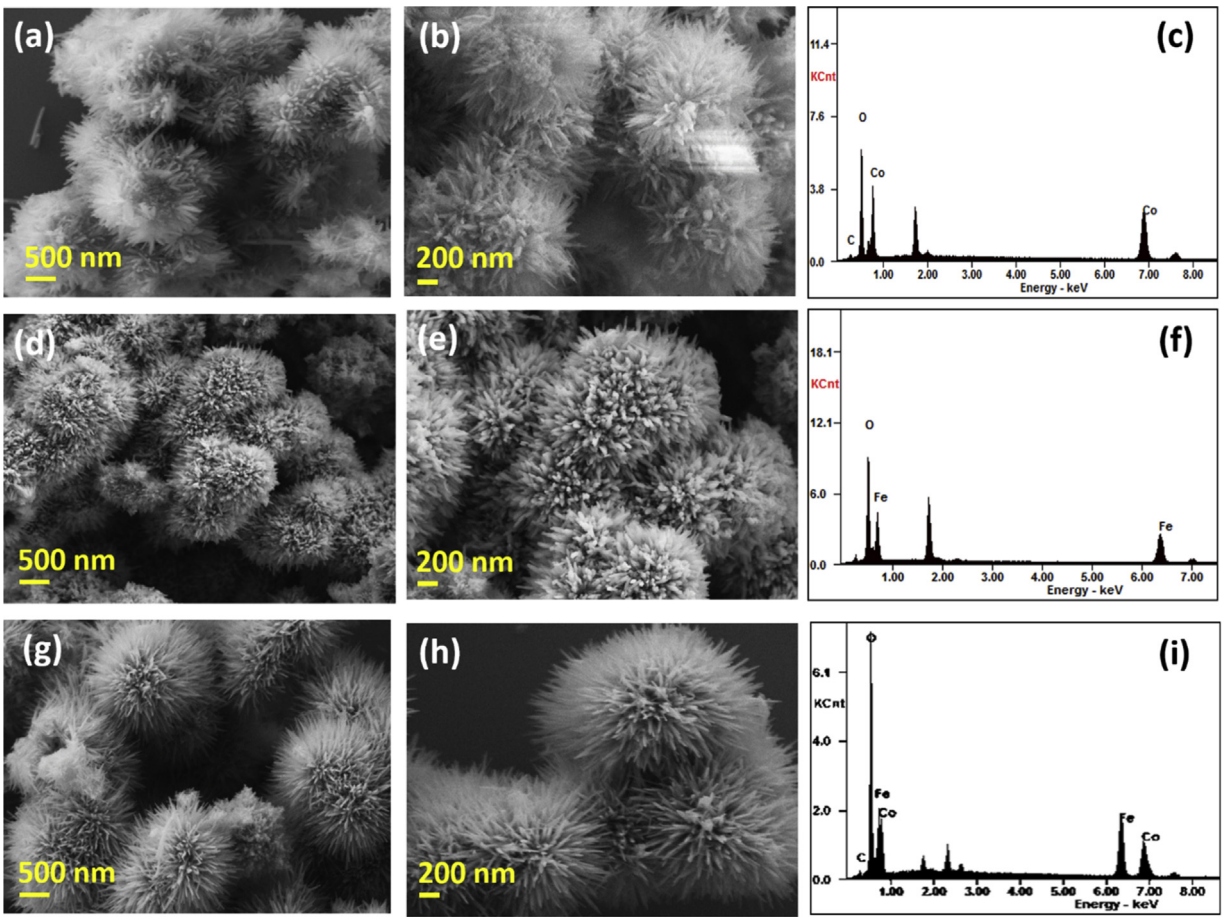

Fig. 2. FE-SEM images at different magnifications of (a and b) Co Oxide/CSs, (d and e) Fe Oxide/CSs, and (g and h) FeCo Oxide/CSs; EDAX analysis of (c) Co Oxide/CSs, (f) Fe Oxide/CSs, and (i) FeCo Oxide/CSs hybrid.

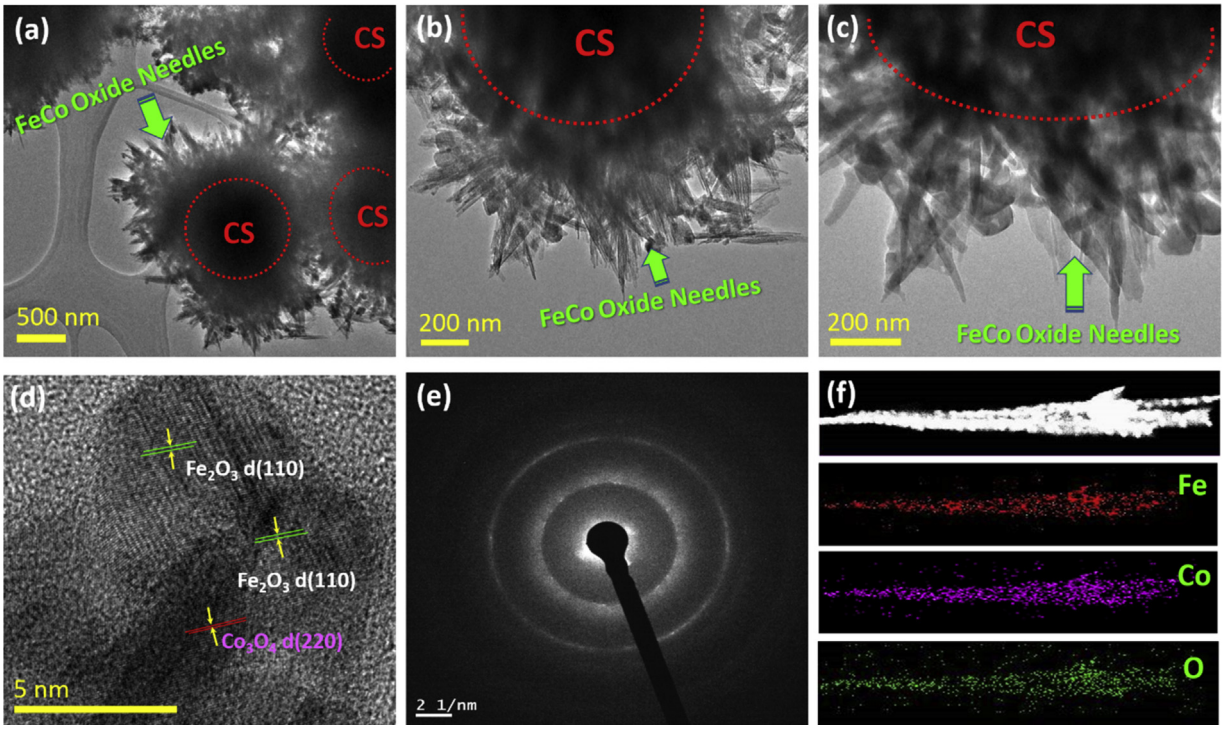

Fig. 3. (a–c) TEM image of FeCo Oxide/CSs hybrid; (d) HR-TEM image and (e) SAED spectrum of FeCo Oxide nanoneedle; (f) STEM-EDS color mapping for Fe, Co, and O in FeCo Oxide/CSs hybrid.

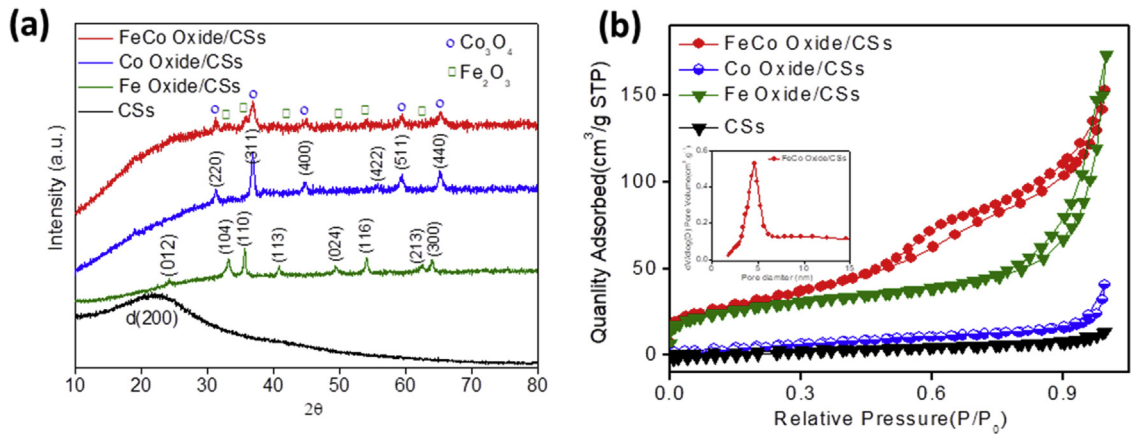

Fig. 4. (a) XRD patterns and (b) Nitrogen adsorption-desorption isotherms of different materials: CSs, Fe Oxide/CSs, Co Oxide/CSs, and FeCo Oxide/CSs hybrid (Inset: pore distribution of the FeCo Oxide/CSs hybrid).

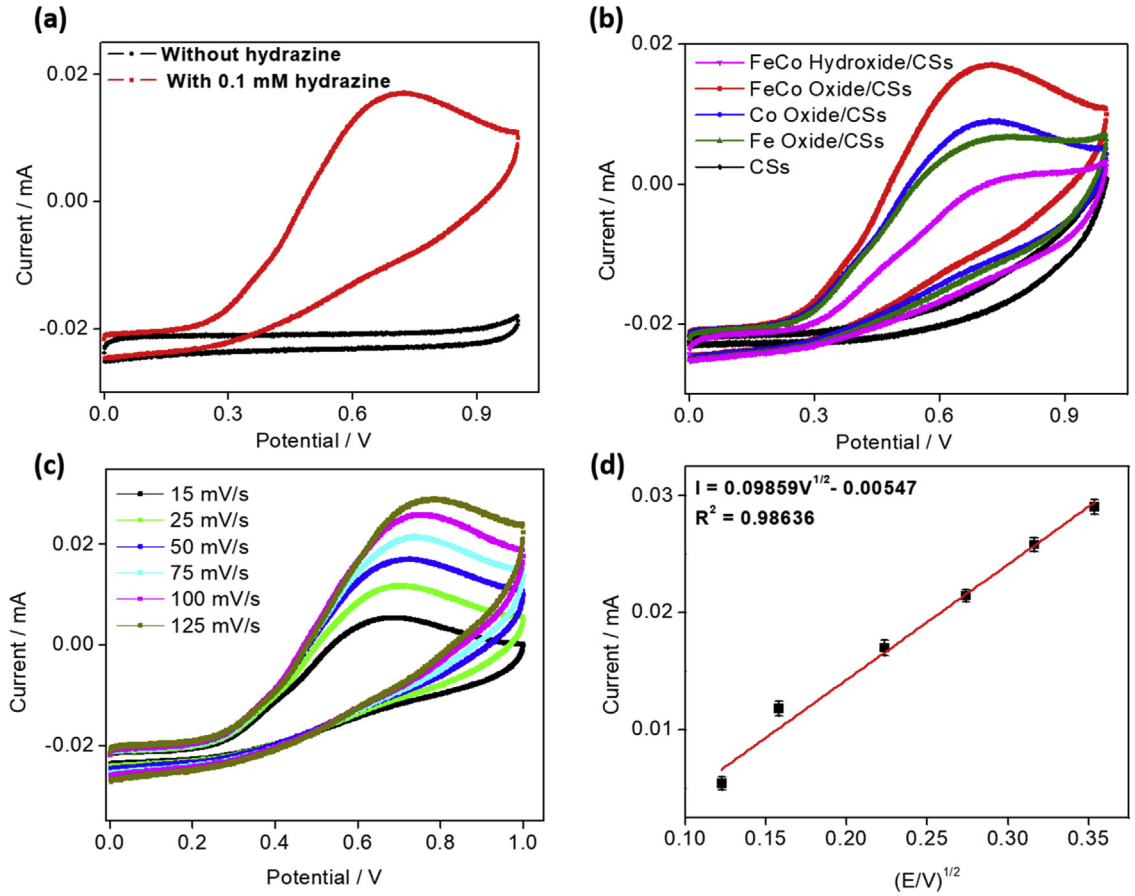

Fig. 5. (a) The CV curves of FeCo Oxide/CSs-modified GCE with the absence and presence of 0.1 mM hydrazine in 0.1 M PBS solution at a scan rate of 50 mV/s; (b) The CV comparison for different modified electrodes in 0.1 M PBS solution with the presence of 0.1 mM hydrazine at a scan rate of 50 mV/s; (c) The CV curves of the FeCo Oxide/CSs-modified GCE in 0.1 M PBS solution with the presence of 0.1 mM hydrazine at different scan rates; (d) The regression curve based on current response *vs.* square root of the scan rate.

dation on the FeCo Oxide/CSs may be attributed to some main following reasons. Firstly, the formation of urchin-like structure increases the surface area, electrical conductivity, and massive channels for diffusion and mass transfer ability. Secondly, the combination between Fe-Co-O at atomic scale to form a mixed oxide nanostructure leads to modulation of electronic structure for individual component, thereby creating enhanced electroactive sites on surface to accelerate the adsorption of reactant and subsequently catalyze the oxidation reaction. The possible electro-oxidation mechanism of hydrazine on the FeCo Oxide/CSs can be illustrated by following Equations: [54]

$$N_2H_4+H_2O <=> N_2H_3+H_3O^+ +e^- (\text{rate-determiningstep}) \quad (1)$$

$$N_2H_3+3H_2O <=> N_2+3H_3O^+ +3e^- (\text{faststep}) \quad (2)$$

The CV measurements of the FeCo Oxide/CSs-modified GCE was tested in 0.1 M PBS solution containing 0.1 mM hydrazine at different scan rates from 15 to 125 mV/s. It can be seen the peak current intensity increases with the rise of the scan rate, as shown in Fig. 5c.

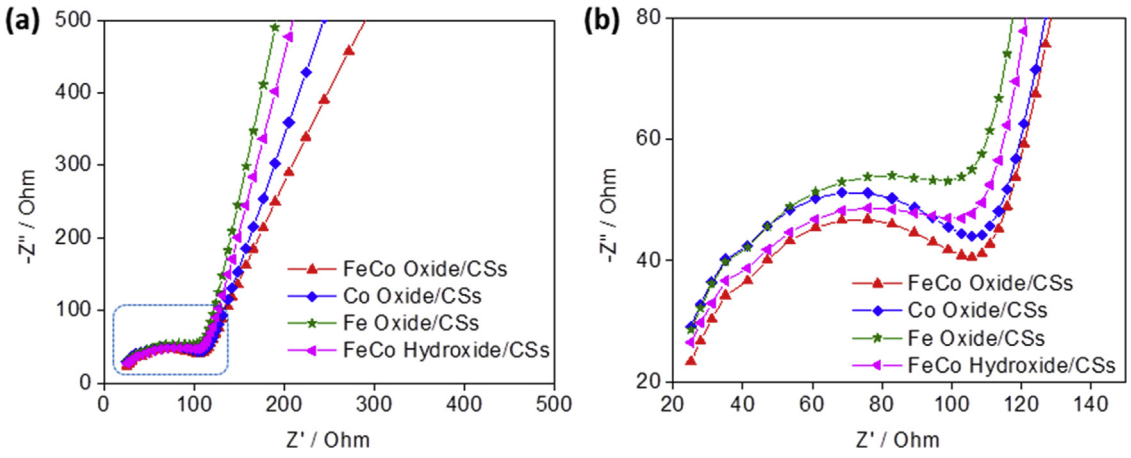

Fig. 6. (a) The EIS measurements of different materials in 0.1 M PBS solution with the frequency range from 10^5 to 10^{-1} ; (b) High magnification of the semicircle parts from EIS curves of different materials.

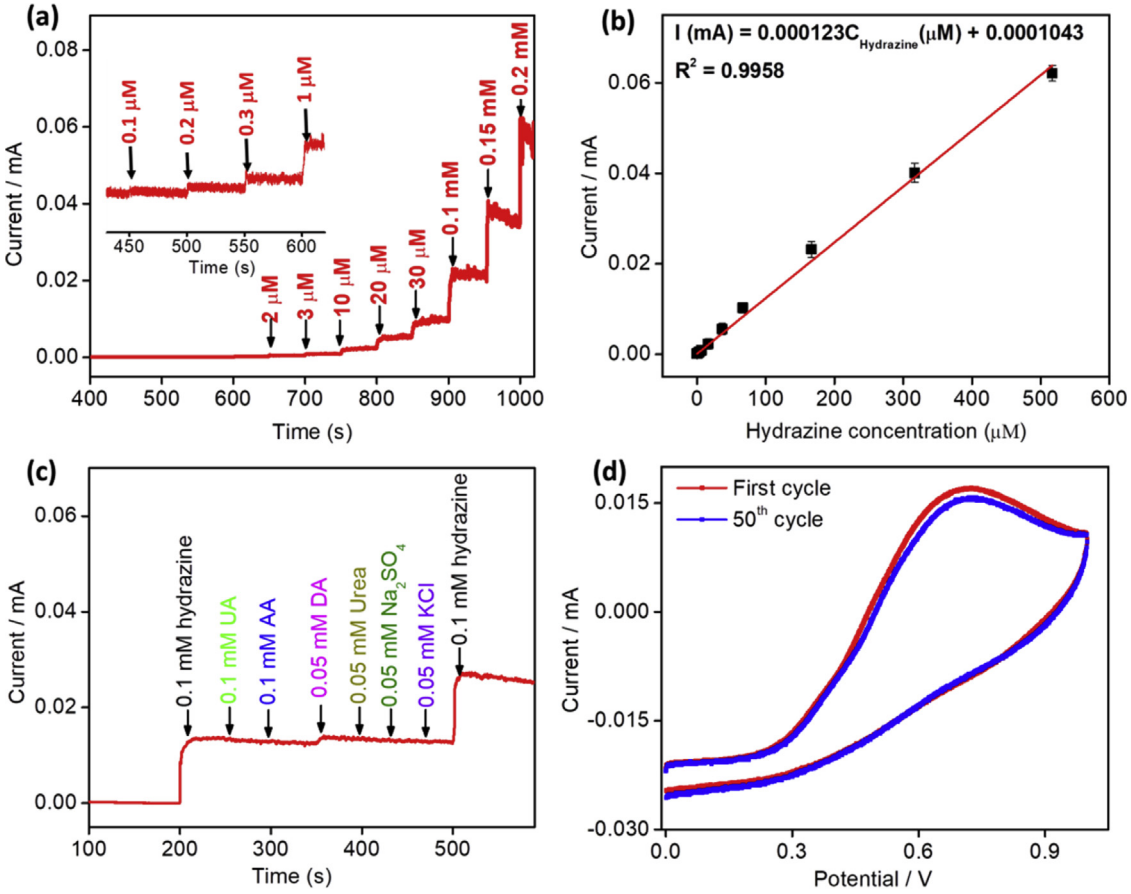

Fig. 7. (a) Amperometric (i–t) curve of the FeCo Oxide/CSs-modified GCE in 0.1 M PBS solution with successive addition of different hydrazine concentrations; (b) The regression curve based on current response *vs.* hydrazine concentration; (c) The selectivity of the FeCo Oxide/CSs-modified GCE with injection of 0.1 mM hydrazine and different interferents; (d) The durability of FeCo Oxide/CSs-modified GCE in 0.1 M PBS solution containing 0.1 mM hydrazine after 50 CV cycles at a scan rate of 50 mV/s.

Fig. 5d displays the corresponding linear fitting curve according to the current response *vs* root square of the scan rate. It shows a good linear relationship consistent with an equation I (mA) = $0.0986V^{1/2}$ - 0.00547 (correlation coefficient of 0.98636), suggesting that the electrochemical oxidation of hydrazine on the FeCo Oxide/CSs-modified GCE is a diffusion-controlled reaction [55].

EIS technique is a powerful method to partially explain the enhanced catalytic activity of the FeCo Oxide/CSs through assessment of the change transfer ability at interfacial area between electrode and electrolyte. Fig. 6a shows the EIS curves of the Fe Oxide/CSs, Co Oxide/CSs, FeCo Hydroxide/CSs, and FeCo Oxide/CSs hybrid. The semicircle part of the EIS result at high frequency range is correlated to the electron transfer resistance (R_{ct}) of electrode at interfacial region. It was found that the Fe Oxide/CSs, Co Oxide/CSs, FeCo Hydroxide/CSs and FeCo Oxide/CSs-modified GCE possess R_{ct} values of 118, 95, 113, and 90 Ω, respectively (Fig. 6b). The R_{ct} value of the FeCo Oxide/CSs-modified GCE is much smaller than other surveyed electrodes. Therefore, we can conclude that the

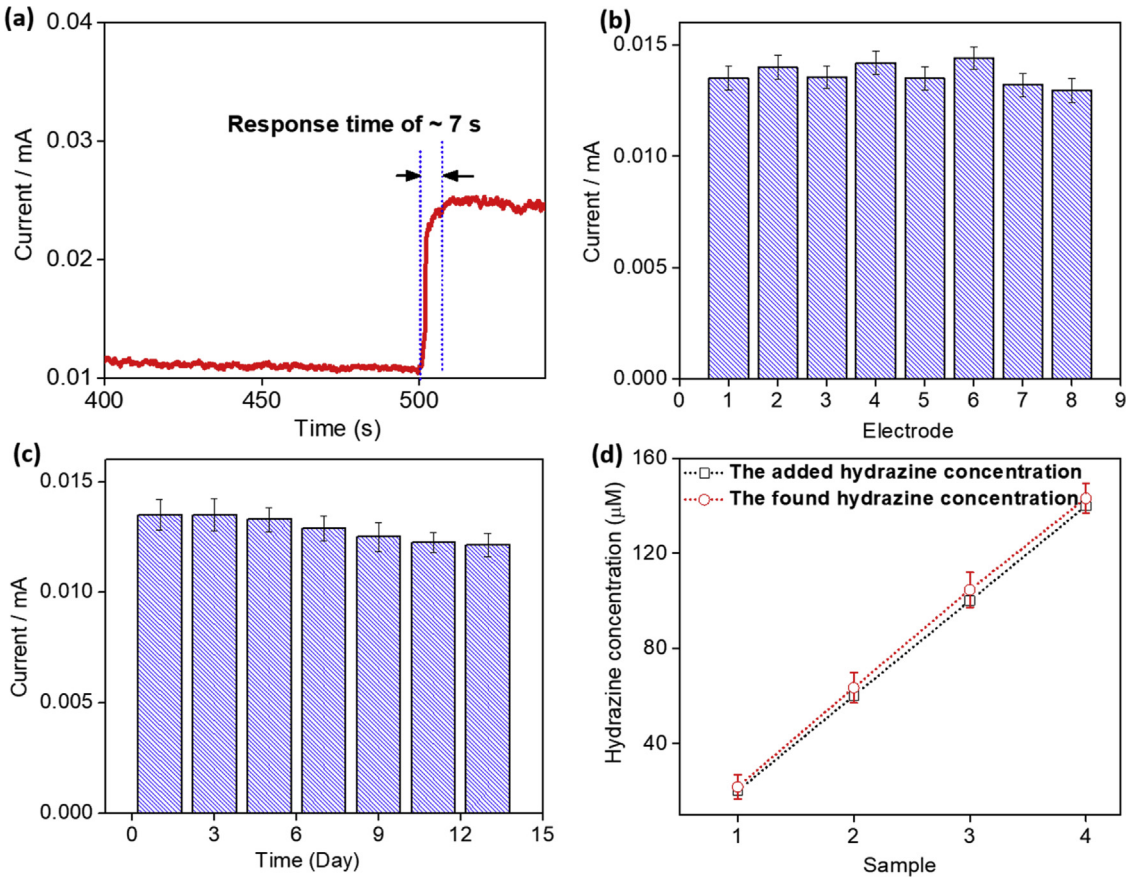

Fig. 8. (a) Response time of the FeCo Oxide/CSs-modified GCE with the addition of 0.1 mM hydrazine; (b) The repeatability of different FeCo Oxide/CSs-modified GCE towards 0.1 mM hydrazine; (c) The storage stability of the FeCo Oxide/CSs-modified GCE; (d) The practical detection of different hydrazine concentrations in 0.1 mM PBS solution with river water containing different known hydrazine concentrations.

FeCo Oxide/CSs-modified GCE has good electrical transfer ability, one of the main reasons for enhancing the electrocatalytic behavior of hybrid towards hydrazine detection.

In order to determine the linear detection range and limit of detection (LOD) of the proposed sensor towards hydrazine detection, the amperometric technique was applied at a working potential of +0.8 V. Fig. 7a exhibits the amperometric response curves of the FeCo Oxide/CSs-modified GCE against successive addition of different hydrazine concentrations into 0.1 M PBS solution. The current rapidly increases with the hydrazine addition, indicating fast-response performance of the proposed sensor for hydrazine detection. Fig. 7b displays a corresponding calibration curve of $I(mA) = 0.000123C_{Hydrazine}$ (μM) + 0.0001043 consistent with a correlation coefficient of 0.9958 for hydrazine detection, which shows a linear detection range from 0.1 μM to 516.6 μM. When the addition of hydrazine concentration into PBS solution more than 0.2 mM, the current response gradually reduces, and therefore, they do not have linear relationship. This is due to the intermediate's adsorption on reactive sites, slow diffusion possibility, and local pH change. The LOD value of the electrode was found to be 0.1 μM according to the S/N = 3. The achieved results imply that the electrochemical performance of the FeCo Oxide/CSs-modified GCE exhibit good catalytic activity for hydrazine detection. This is further demonstrated when its performance is compared to other previous reports, as shown in Table 1.

Selectivity is also an important factor for sensing hydrazine, thus the anti-interference analysis of the FeCo Oxide/CSs-modified GCE towards various interferences was investigated (Fig. 7c). The selectivity of the FeCo Oxide/CSs-modified GCE was measured with the addition of some common interferences, such as ascorbic acid (0.1 mM), uric acid (0.1 mM), urea (0.05 mM), dopamine (0.05 mM), Na_2SO_4 (0.05 mM), and KCl (0.05 mM). In this context, 0.1 M PBS solution was initially added with 0.1 mM hydrazine followed by the continuous addition of AA, UA, DA, urea, KCl, and Na_2SO_4 under magnetic stirring. It can be seen that the initial addition of 0.1 mM hydrazine leads to a strong current response. Meanwhile, the subsequent additions of interferences produce weak current responses, which are almost negligible. Furthermore, the final addition of 0.1 mM hydrazine still retain current response similar to its first-time addition, implying that the modified electrode shows excellent selectivity for hydrazine detection.

As important parameters to decide the practical application of a biosensor, the durability and stability were also examined. In this context, the durability of the FeCo Oxide/CSs-modified GCE was carried out through evaluating the CV response over a long-term cycling in 0.1 M PBS solution with the presence of 0.1 mM hydrazine. As shown in Fig. 7d, the shape and current response after 50 cycles still retain similar feature of its original curve, suggesting the good durability of the FeCo Oxide/CSs-modified GCE. Furthermore, the amperometric measurement of the FeCo Oxide/CSs-modified GCE was conducted with the addition of 0.1 mM hydrazine for long-term amperometric operation. Figure S2 indicates the current response has the retention of 91.3% after 300 s, implying appropriate stability of the sensor towards hydrazine detection. The small decrease of current response for the FeCo Oxide/CSs after prolonged testing may be resulted from certain degradation of urchin structures due to effect of ion diffusion and electrolyte penetration during long-term reaction. This is confirmed by a SEM image of the material after stability test (Fig. S3), which indicates some morphological changes with little reduction

Table 1
Comparison of sensing performance between the FeCo Oxide/CSs-modified GCE and previous reports towards hydrazine detection.

Materials	LOD (μM)	Detection range (μM)	References
PEDOT:PSS/Pd	0.12	0.4–100	[56]
Nano-CoTAPC/SPEs	30	10-100	[57]
ZnO/SWCNT	0.1	0.5-50	[58]
Hierarchical micro/nano architectures/ZnO	0.51	0.8-200	[59]
TiO_2/CNT	0.22	0.35-162	[60]
α-Fe_2O_3/CPANI nanocomposite	0.153	0.2-40	[54]
AuPd nanorod chains	0.02	0.10-501	[61]
Cu_xO–PEDOT	0.2	0.5–600	[62]
Mesoporous Au/ZnO	0.242	0.2–14.2	[63]
ZnO/MWCNTs/GCE	0.18	0.6-250	[64]
Au/SWCNHs/GCE	1.1	5-3345	[65]
FeCo Oxide/CSs	0.1	0.1- 516.6	This study

of uniformity, density, and sharpness of nanoneedles in the urchin structures, thereby leading to decreasing electrocatalytic active site number for hydrazine oxidation.

In another regard, the response time was evaluated to be 7 s, implying fast response of the developed FeCo Oxide/CSs-modified GCE towards hydrazine oxidation (Fig. 8a). The reproducibility and storage stability of the FeCo Oxide/CSs-modified GCE were also examined in detail. In this regard, the current responses of eight different electrodes in 0.1 M PBS solution containing 0.1 mM hydrazine exhibit the relative standard deviation (RSD) of 3.63%, implying its good reproducibility (Fig. 8b). The current sensor was investigated the stability after storing at room temperature for long-term time. The obtained results indicate that it retains a current value of about 89.8% compared to initial response for hydrazine detection after 13 days, indicating its good storage stability (Fig. 8c). Furthermore, to evaluate the feasibility of the proposed sensor for practical detection of hydrazine, four river water samples containing different known hydrazine concentrations were spiked in 0.1 M PBS solution and were then used to detect hydrazine under the optimized conditions (Fig. 8d). The sensor shows the satisfactory results with the RSD% of 3.8–5.6% and the recovery of 102.3–108.5%, suggesting its possibility for practical hydrazine sensing application.

4. Conclusion

In this study, we successfully developed a novel urchin-like structure of FeCo Oxide/CSs hybrid through a facile two-step hydrothermal method followed by an annealing at 300 °C in air. The formation of such unique structure was highly beneficial for electroactive sites, charge transfer, and diffusion ability to improve electrochemical oxidation of hydrazine. The proposed FeCo Oxide/CSs-based sensor can electrochemically detect hydrazine with wide linear range detection range of 0.1–516.6 μM, low LOD of 0.1 μM, and fast response time of 7 s. In addition, the good anti-interference was also demonstrated. Furthermore, the sensor could accurately determinate hydrazine in real samples. The achieved results imply that the FeCo Oxide/CSs can be applied as an efficient catalyst towards sensitive hydrazine detection for practical sensing applications.

Acknowledgments

The authors acknowledge support from the fund of Duy Tan University in Da Nang city and Ton Duc Thang University in Ho Chi Minh city, Viet Nam.

Appendix A. Supplementary data

Supplementary material related to this article can be found, in the online version, at doi:https://doi.org/10.1016/j.jpba.2019.04.008.

References

[1] K. Asazawa, K. Yamada, H. Tanaka, M. Taniguchi, K. Oguro, Electrochemical oxidation of hydrazine and its derivatives on the surface of metal electrodes in alkaline media, J. Power Sources 191 (2009) 362–365, http://dx.doi.org/10.1016/j.jpowsour.2009.02.009.
[2] M.M. Rahman, J. Ahmed, A.M. Asiri, I.A. Siddiquey, M.A. Hasnat, Development of highly-sensitive hydrazine sensor based on facile CoS2-CNT nanocomposites, RSC Adv. 6 (2016) 90470–90479, http://dx.doi.org/10.1039/c6ra08772h.
[3] M.M. Rahman, B.M. Abu-Zied, A.M. Asiri, Ultrasensitive hydrazine sensor fabrication based on Co-doped ZSM-5 zeolites for environmental safety, RSC Adv. 7 (2017) 21164–21174, http://dx.doi.org/10.1039/C7RA00952F.
[4] Q. Zhai, W. Feng, G. Feng, Rapid detection of hydrazine in almost wholly water solution and in living cells with a new colorimetric and fluorescent turn-on probe, Anal. Methods 8 (2016) 5832–5837, http://dx.doi.org/10.1039/c6ay01367h.
[5] B. Shi, S. Qi, M. Yu, C. Liu, Z. Li, L. Wei, Z. Ni, Colorimetric and fluorescent detection of hydrazine with high sensitivity and excellent selectivity, Spectrochim. Acta - Part A Mol. Biomol. Spectrosc. 188 (2018) 208–212, http://dx.doi.org/10.1016/j.saa.2017.07.003.
[6] L. Cui, Z. Peng, C. Ji, J. Huang, D. Huang, J. Ma, S. Zhang, X. Qian, Y. Xu, Hydrazine detection in the gas state and aqueous solution based on the Gabriel mechanism and its imaging in living cells, Chem. Commun. 50 (2014) 1485–1487, http://dx.doi.org/10.1039/c3cc48304e.
[7] Y. Ding, S. Zhao, Q. Wang, X. Yu, W. Zhang, Construction of a coumarin based fluorescent sensing platform for palladium and hydrazine detection, Sens. Actuators B-Chem. 256 (2018) 1107–1113, http://dx.doi.org/10.1016/j.snb.2017.10.119.
[8] P.K. Kannan, S.A. Moshkalev, C.S. Rout, Electrochemical sensing of hydrazine using multilayer graphene nanobelts, RSC Adv. 6 (2016) 11329–11334, http://dx.doi.org/10.1039/c5ra24912k.
[9] Z. Wei, Z. Hai, M.K. Akbari, J. Hu, L. Hyde, S. Depuydt, F. Verpoort, S. Zhuiykov, Ultrasensitive, sustainable, and selective electrochemical hydrazine detection by ALD-developed two-dimensional WO3, ChemElectroChem. 5 (2018) 266–272, http://dx.doi.org/10.1002/celc.201700968.
[10] G. Maduraiveeran, R. Ramaraj, Gold nanoparticle-based sensing platform of hydrazine, sulfite, and nitrite for food safety and environmental monitoring, J. Anal. Sci. Technol. 8 (2017) 14, http://dx.doi.org/10.1186/s40543-017-0113-1.
[11] A.A. Ensafi, M.M. Abarghoui, B. Rezaei, Facile synthesis of Pt-Cu@silicon nanostructure as a new electrocatalyst supported matrix, electrochemical detection of hydrazine and hydrogen peroxide, Electrochim. Acta 190 (2016) 199–207, http://dx.doi.org/10.1016/j.electacta.2015.12.180.
[12] Y. Tan, Y. Fu, Q. Xie, D. Yang, H. Xiao, S. Yao, C. Chen, Recent advances in electrochemical glucose biosensors: a review, RSC Adv. 3 (2012) 4473, http://dx.doi.org/10.1039/c2ra22351a.
[13] M.M. Rahman, A.J.S. Ahammad, J.H. Jin, S.J. Ahn, J.J. Lee, A comprehensive review of glucose biosensors based on nanostructured metal-oxides, Sensors 10 (2010) 4855–4886, http://dx.doi.org/10.3390/s100504855.
[14] Y. Zhang, T. Han, Z. Wang, C. Zhao, J. Li, T. Fei, S. Liu, G. Lu, T. Zhang, In situ formation of N-doped carbon film-immobilized Au nanoparticles-coated ZnO jungle on indium tin oxide electrode for excellent high-performance detection of hydrazine, Sens. Actuators B-Chem. 243 (2017) 1231–1239, http://dx.doi.org/10.1016/j.snb.2016.12.085.
[15] Y.J. Yang, W. Li, X. Wu, Copper sulfide|reduced graphene oxide nanocomposite for detection of hydrazine and hydrogen peroxide at low potential in neutral medium, Electrochim. Acta 123 (2014) 260–267, http://dx.doi.org/10.1016/j.electacta.2014.01.046.
[16] X. Chen, H. Wang, H. Wan, T. Wu, D. Shu, L. Shen, Y. Wang, P. Ruterana, P.D. Lund, H. Wang, Core/shell Cu/FePtCu nanoparticles with face-centered tetragonal texture: an active and stable low-Pt catalyst for enhanced oxygen reduction, Nano Energy 54 (2018) 280–287, http://dx.doi.org/10.1016/j.nanoen.2018.10.034.
[17] G. Doria, J. Conde, B. Veigas, L. Giestas, C. Almeida, M. Assunção, J. Rosa, P.V. Baptista, Noble metal nanoparticles for biosensing applications, Sensors 12 (2012) 1657–1687, http://dx.doi.org/10.3390/s120201657.

[18] J. Tang, D. Tang, Non-enzymatic electrochemical immunoassay using noble metal nanoparticles: a review, Microchim. Acta 182 (2015) 2077–2089, http://dx.doi.org/10.1007/s00604-015-1567-8.
[19] X. Li, J. Shan, W. Zhang, S. Su, L. Yuwen, L. Wang, Recent advances in synthesis and biomedical applications of two-dimensional transition metal dichalcogenide nanosheets, Small. 13 (2017) 1–18, http://dx.doi.org/10.1002/smll.201602660.
[20] L. Zhu, W. Zeng, Room-temperature gas sensing of ZnO-based gas sensor: a review, Sens. Actuators A-Phys. 267 (2017) 242–261, http://dx.doi.org/10.1016/j.sna.2017.10.021.
[21] M. Pumera, A.H. Loo, Layered transition-metal dichalcogenides (MoS2 and WS2) for sensing and biosensing, TrAC - Trends Anal. Chem. 61 (2014) 49–53, http://dx.doi.org/10.1016/j.trac.2014.05.009.
[22] W. Choi, N. Choudhary, G.H. Han, J. Park, D. Akinwande, Y.H. Lee, Recent development of two-dimensional transition metal dichalcogenides and their applications, Mater. Today 20 (2017) 116–130, http://dx.doi.org/10.1016/j.mattod.2016.10.002.
[23] Y.H. Wang, K.J. Huang, X. Wu, Recent advances in transition-metal dichalcogenides based electrochemical biosensors: a review, Biosens. Bioelectron. 97 (2017) 305–316, http://dx.doi.org/10.1016/j.bios.2017.06.011.
[24] L. Chen, T. Wang, Y. Xue, X. Zhou, J. Zhou, X. Cheng, Z. Xie, Q. Kuang, L. Zheng, Rationally armoring PtCu Alloy with metal-organic frameworks as highly selective nonenzyme electrochemical sensor, Adv. Mater. Interfaces (2018) 1801168, http://dx.doi.org/10.1002/admi.201801168, 1801168.
[25] D. Zhao, G. Yu, K. Tian, C. Xu, A highly sensitive and stable electrochemical sensor for simultaneous detection towards ascorbic acid, dopamine, and uric acid based on the hierarchical nanoporous PtTi alloy, Biosens. Bioelectron. 82 (2016) 119–126, http://dx.doi.org/10.1016/j.bios.2016.03.074.
[26] Q. Liu, H. Wang, X. Wang, R. Tong, X. Zhou, X. Peng, H. Wang, H. Tao, Z. Zhang, Bifunctional Ni1−xFex layered double hydroxides/Ni foam electrodes for high-efficient overall water splitting: a study on compositional tuning and valence state evolution, Int. J. Hydrogen Energy 42 (2017) 5560–5568, http://dx.doi.org/10.1016/j.ijhydene.2016.06.056.
[27] L. Li, X. Liu, C. Liu, H. Wan, J. Zhang, P. Liang, H. Wang, H. Wang, Ultra-long life nickel nanowires@nickel-cobalt hydroxide nanoarrays composite pseudocapacitive electrode: construction and activation mechanism, Electrochim. Acta 259 (2018) 303–312, http://dx.doi.org/10.1016/j.electacta.2017.10.190.
[28] H. Wan, L. Li, Y. Xu, Q. Tan, X. Liu, J. Zhang, H. Wang, H. Wang, Three-dimensional cotton-like nickel nanowire@Ni–Co hydroxide nanosheet arrays as binder-free electrode for high-performance asymmetric supercapacitor, Nanotechnology 29 (2018), 194003.
[29] B.G. Kim, H.J. Kim, S. Back, K.W. Nam, Y. Jung, Y.K. Han, J.W. Choi, Improved reversibility in lithium-oxygen battery: understanding elementary reactions and surface charge engineering of metal alloy catalyst, Sci. Rep. 4 (2015) 18–21, http://dx.doi.org/10.1038/srep04225.
[30] Q. Tang, J. Duan, Y. Duan, B. He, L. Yu, Recent advances in alloy counter electrodes for dye-sensitized solar cells. A critical review, Electrochim. Acta 178 (2015) 886–899, http://dx.doi.org/10.1016/j.electacta.2015.08.072.
[31] K. Ramachandran, T. Raj Kumar, K.J. Babu, G. Gnana Kumar, Ni-Co bimetal nanowires filled multiwalled carbon nanotubes for the highly sensitive and selective non-enzymatic glucose sensor applications, Sci. Rep. 6 (2016) 1–12, http://dx.doi.org/10.1038/srep36583.
[32] M.S. Balogun, Y. Luo, W. Qiu, P. Liu, Y. Tong, A review of carbon materials and their composites with alloy metals for sodium ion battery anodes, Carbon 98 (2016) 162–178, http://dx.doi.org/10.1016/j.carbon.2015.09.091.
[33] S. Diyarbakir, H. Can, Ö. Metin, Reduced graphene oxide-supported cupd alloy nanoparticles as efficient catalysts for the sonogashira cross-coupling reactions, ACS Appl. Mater. Interfaces 7 (2015) 3199–3206, http://dx.doi.org/10.1021/am507764u.
[34] D.Y. Wang, M. Gong, H.L. Chou, C.J. Pan, H.A. Chen, Y. Wu, M.C. Lin, M. Guan, J. Yang, C.W. Chen, Y.L. Wang, B.J. Hwang, C.C. Chen, H. Dai, Highly active and stable hybrid catalyst of cobalt-doped FeS<inf>2</inf> nanosheets-carbon nanotubes for hydrogen evolution reaction, J. Am. Chem. Soc. 137 (2015) 1587–1592, http://dx.doi.org/10.1021/ja511572q.
[35] Y.J. Wang, N. Zhao, B. Fang, H. Li, X.T. Bi, H. Wang, Carbon-supported Pt-Based alloy electrocatalysts for the oxygen reduction reaction in polymer electrolyte membrane fuel cells: particle size, shape, and composition manipulation and their impact to activity, Chem. Rev. 115 (2015) 3433–3467, http://dx.doi.org/10.1021/cr500519c.
[36] G. Khadra, A. Tamion, F. Tournus, O. Boisron, C. Albin, V. Dupuis, Structure and magnetic properties of FeCo clusters: carbon environment and annealing effects, J. Phys. Chem. C 121 (2017) 10713–10718, http://dx.doi.org/10.1021/acs.jpcc.6b10715.
[37] L. Liardet, J.E. Katz, J. Luo, M. Grätzel, X. Hu, An ultrathin cobalt–iron oxide catalyst for water oxidation on nanostructured hematite photoanodes, J. Mater. Chem. A 7 (2019) 6012–6020, http://dx.doi.org/10.1039/C8TA12295D.
[38] S.H. Noh, M.H. Seo, J. Kang, T. Okajima, B. Han, T. Ohsaka, Towards a comprehensive understanding of FeCo coated with N-doped carbon as a stable bi-functional catalyst in acidic media, NPG Asia Mater. 8 (2016) e312–10, http://dx.doi.org/10.1038/am.2016.142.
[39] C.G. Morales-Guio, L. Liardet, X. Hu, Oxidatively electrodeposited thin-film transition metal (oxy)hydroxides as oxygen evolution catalysts, J. Am. Chem. Soc. 138 (2016) 8946–8957, http://dx.doi.org/10.1021/jacs.6b05196.
[40] M.S. Burke, M.G. Kast, L. Trotochaud, A.M. Smith, S.W. Boettcher, Cobalt–iron (Oxy)hydroxide oxygen evolution electrocatalysts: the role of structure and composition on activity, stability, and mechanism, J. Am. Chem. Soc. 137 (2015) 3638–3648, http://dx.doi.org/10.1021/jacs.5b00281.
[41] W.W. Liu, S.P. Chai, A.R. Mohamed, U. Hashim, Synthesis and characterization of graphene and carbon nanotubes: a review on the past and recent developments, J. Ind. Eng. Chem. 20 (2014) 1171–1185, http://dx.doi.org/10.1016/j.jiec.2013.08.028.
[42] D. Li, H. Chen, G. Liu, M. Wei, L.X. Ding, S. Wang, H. Wang, Porous nitrogen doped carbon sphere as high performance anode of sodium-ion battery, Carbon 94 (2015) 888–894, http://dx.doi.org/10.1016/j.carbon.2015.07.067.
[43] S. Li, A. Pasc, V. Fierro, A. Celzard, Hollow carbon spheres, synthesis and applications-a review, J. Mater. Chem. A 4 (2016) 12686–12713, http://dx.doi.org/10.1039/c6ta03802f.
[44] M.W. Dlamini, D.O. Kumi, T.N. Phaahlamohlaka, A.S. Lyadov, D.G. Billing, L.L. Jewell, N.J. Coville, Carbon spheres prepared by hydrothermal synthesis - a support for bimetallic Iron cobalt Fischer-Tropsch catalysts, ChemCatChem 7 (2015) 3000–3011, http://dx.doi.org/10.1002/cctc.201500334.
[45] J.C. Claussen, M.A. Daniele, J. Geder, M. Pruessner, A.J. Mäkinen, B.J. Melde, M. Twigg, J.M. Verbarg, I.L. Medintz, Platinum-paper micromotors: an urchin-like nanohybrid catalyst for green monopropellant bubble-thrusters, ACS Appl. Mater. Interfaces 6 (2014) 17837–17847, http://dx.doi.org/10.1021/am504525e.
[46] H. Yang, Y. Zhang, F. Hu, Q. Wang, Urchin-like CoP nanocrystals as hydrogen evolution reaction and oxygen reduction reaction dual-electrocatalyst with superior stability, Nano Lett. 15 (2015) 7616–7620, http://dx.doi.org/10.1021/acs.nanolett.5b03446.
[47] Z. Zhang, Y. Wang, S. Chou, H. Li, H. Liu, Rapid synthesis of a -Fe2O3/rGO nanocomposites by microwave autoclave as superior anodes for sodium-ion batteries, J. Power Sources 280 (2015) 107–113, http://dx.doi.org/10.1016/j.jpowsour.2015.01.092.
[48] F. Zhang, C. Yuan, X. Lu, L. Zhang, Q. Che, X. Zhang, Facile growth of mesoporous Co 3 O 4 nanowire arrays on Ni foam for high performance electrochemical capacitors, J. Power Sources 203 (2012) 250–256, http://dx.doi.org/10.1016/j.jpowsour.2011.12.001.
[49] V. Etacheri, C. Wang, M.J. O'Connell, C.K. Chan, V.G. Pol, Porous carbon sphere anodes for enhanced lithium-ion storage, J. Mater. Chem. A 3 (2015) 9861–9868, http://dx.doi.org/10.1039/c5ta01360g.
[50] E. Method, R. Han, W. Li, W. Pan, M. Zhu, D. Zhou, F. Li, 1D magnetic materials of Fe 3 O 4 and Fe with high performance of microwave absorption fabricated by electrospinning method, Sci. Rep. 4 (2014) 7493, http://dx.doi.org/10.1038/srep07493.
[51] T.H. Yoon, Y.J. Park, Carbon nanotube / Co 3 O 4 composite for air electrode of lithium-air battery, Nanoscale Res. Lett. 7 (2012) 28, http://dx.doi.org/10.1186/1556-276X-7-28.
[52] L. An, N. Jiang, B. Li, S. Hua, Y. Fu, J. Liu, W. Hao, D. Xia, Z. Sun, A highly active and durable iron/cobalt alloy catalyst encapsulated in N-doped graphitic carbon nanotubes for oxygen reduction reaction by a nanofibrous dicyandiamide template, J. Mater. Chem. A 6 (2018) 5962–5970, http://dx.doi.org/10.1039/c8ta01247d.
[53] X. Wang, R. Rinaldi, Bifunctional Ni catalysts for the one-pot conversion of Organosolv lignin into cycloalkanes, Catal. Today 269 (2016) 48–55, http://dx.doi.org/10.1016/j.cattod.2015.11.047.
[54] F.A. Harraz, A.A. Ismail, S.A. Al-sayari, A. Al-hajry, M.S. Al-assiri, Highly sensitive amperometric hydrazine sensor based on novel α-Fe 2 O 3 / crosslinked polyaniline nanocomposite modified glassy carbon electrode, Sens. Actuators B-Chem. 234 (2016) 573–582, http://dx.doi.org/10.1016/j.snb.2016.05.021.
[55] T. Choi, S.H. Kim, C.W. Lee, H. Kim, S.K. Choi, S.H. Kim, E. Kim, J. Park, H. Kim, Synthesis of carbon nanotube-nickel nanocomposites using atomic layer deposition for high-performance non-enzymatic glucose sensing, Biosens. Bioelectron. 63 (2015) 325–330, http://dx.doi.org/10.1016/j.bios.2014.07.059.
[56] E.G. Tolstopjatova, V.V. Kondratiev, S.N. Eliseeva, Multi-layer PEDOT:PSS/Pd composite electrodes for hydrazine oxidation, J. Solid State Electrochem. 19 (2015) 2951–2959, http://dx.doi.org/10.1007/s10008-015-2907-7.
[57] C.W. Foster, J. Pillay, J.P. Metters, C.E. Banks, Cobalt phthalocyanine modified electrodes utilised in electroanalysis: Nano-structured modified electrodes vs. Bulk modified screen-printed electrodes, Sensors 14 (2014) 21905–21922, http://dx.doi.org/10.3390/s141121905.
[58] K.N. Han, C.A. Li, M.P.N. Bui, X.H. Pham, G.H. Seong, Control of ZnO morphologies on carbon nanotube electrodes and electrocatalytic characteristics toward hydrazine, Chem. Commun. 47 (2011) 938–940, http://dx.doi.org/10.1039/c0cc03848b.
[59] Y. Ni, J. Zhu, L. Zhang, J. Hong, Hierarchical ZnO micro/nanoarchitectures: hydrothermal preparation, characterization and application in the detection of hydrazine, CrystEngComm 12 (2010) 2213–2218, http://dx.doi.org/10.1039/b923857n.
[60] S.P. Kim, H.C. Choi, Reusable hydrazine amperometric sensor based on Nafion ® -coated TiO 2 – carbon nanotube modified electrode, Sens. Actuators B-Chem. 207 (2015) 424–429, http://dx.doi.org/10.1016/j.snb.2014.10.029.
[61] Y. Liu, S. Chen, A. Wang, J. Feng, X. Wu, X. Weng, An ultra-sensitive electrochemical sensor for hydrazine based on AuPd nanorod alloy nanochains, Electrochim. Acta 195 (2016) 68–76, http://dx.doi.org/10.1016/j.electacta.2016.01.229.
[62] F. Xu, Y. Liu, L. Wang, Electrochemical preparation of a three dimensional PEDOT – Cu x O hybrid for enhanced oxidation and sensitive detection of hydrazine, Anal. Methods 8 (2016) 316–325, http://dx.doi.org/10.1039/c5ay02465j.

[63] A.A. Ismail, F.A. Harraz, M. Faisal, A.M. El-toni, A. Al-hajry, M.S. Al-assiri, A sensitive and selective amperometric hydrazine sensor based on mesoporous Au/ZnO nanocomposites, JMADE 109 (2016) 530–538, http://dx.doi.org/10.1016/j.matdes.2016.07.107.
[64] B. Fang, C. Zhang, W. Zhang, G. Wang, A novel hydrazine electrochemical sensor based on a carbon nanotube-wired ZnO nanoflower-modified electrode, Electrochim. Acta 55 (2009) 178–182, http://dx.doi.org/10.1016/j.electacta.2009.08.036.
[65] S. Zhao, L. Wang, T. Wang, Q. Han, S. Xu, A high-performance hydrazine electrochemical sensor based on gold nanoparticles / single-walled carbon nanohorns composite film, Appl. Surf. Sci. 369 (2016) 36–42, http://dx.doi.org/10.1016/j.apsusc.2016.02.013.